

Spatio-temporal dynamics of outbreak on a lattice with quenched mobility patterns

Jozef Černák*

December 23, 2021

Department of Nuclear and Sub-Nuclear Physics, Faculty of Science, Institute of Physics, Pavol Jozef Šafárik University in Košice, Košice, Slovak Republic

Abstract

We have designed a computational model of a virus spread near the outbreak threshold. Using computer simulation we studied the Susceptible - Infected - Recovered (SIR) process where in consequence of a force of habit that is manifested by the population mobility patterns, the recovered persons create the spatio-temporal patterns as the barriers to a virus transmission. The results show a spontaneous stopping of the virus spread without a need to infect the whole population, a non-trivial random noise of daily count of infected cases, and power laws of a cumulative count of infected cases. Outbreak evolution strongly depends on the initial conditions thus we concluded that the model has the features of chaotic systems that makes it difficult to predict its behaviors.

Introduction

The SARS-CoV-2 virus and their variants continue in the evolution in the global space. The destiny of virus extinction is unclear (1) and it depends on many evolutionary factors

*jozefcernak@gmail.com

(2). An increase of social distance is a measure to slow down the pandemic. It has been successfully demonstrated that either local or national non-pharmaceutical interventions led to a significant reduction of the virus rate transmission on large scales with beneficial and measurable health outcomes (3, 4).

The mathematical models, susceptible-infected-recovered (SIR), susceptible - infected -susceptible (SIS), susceptible - infected - recovered - susceptible (SIRS) and susceptible - exposed - infected - recovered -susceptible (SEIRS) (5, 6), predict an exponential growth of a cumulative count of infected cases $I(t) \sim \exp(t)$, where t is time. Similarly, the SI, SIS, and SIR models on the complex networks show an exponential growth of the number of links available for future transmission (7). These theoretical predictions are in contrast to a cumulative count of infected cases $I(t)$ in China during the beginning of the first SARS-CoV-2 outbreak wave. The first wave in China shows a power law, $I(t) \sim t^\alpha$ (8), where α is an exponent. A deviation from the expected exponential growth models, we consider for a signature of a quite different mechanism of the contagion, than it is widely accepted for traditional SIR or SEIR models (9).

The authors Rhodes and Anderson (10) analyzed distribution of epidemic sizes and epidemic durations of measles outbreaks. They observed that dynamical structures of the measles returns reflect the existence of an underlying scaling mechanism. Random structures often exhibit self-similar geometry that is characterized by a power law (11). So, it is useful to consider a virus contagion as a dynamical process on the fractal networks like a diffusion in the percolating networks (11) as well as the branching process (12) on these networks. Kumamoto and Kamihigashi (13) reviewed mathematical mechanisms that are known to generate the power laws. In particular, they focused on stochastic processes based on growth and preferential attachments including the Yule process, the Simon process, the Barabási - Albert Model, and stochastic models based on geometric Brownian motion.

Stroud et al. (14) introduced the power laws of some variables in the traditional homogeneous models, SIR and SEIR, to better model the real outbreaks. In the stochastic version of the SIR process, the authors Ben-Naim and Krapivsky (15) found nontrivial

scaling relations of a maximal size of outbreak $M \sim N^{\frac{2}{3}}$ and duration of outbreak $T \sim T^{\frac{1}{2}}$ on a population size N near the outbreak threshold.

We observed that the time series of daily count of infected cases $i(t)$ show a noise that is not possible to neither reproduce nor explain by the classical models of epidemic. Hurst investigated annual values of some phenomena such as river discharges, rainfall, temperatures. He observed that these values are approximately normally distributed if no account is taken of order of occurrence. So far as is known, there is no regularity in the occurrence or the length of these periods, and usually there is no significant correlation over one of them between a year and its successor. Hurst considered this phenomenon to be important in problems of storage (16). Mandelbrot found that the Hurst exponent H must be $0 \leq H \leq 1$. If $H < \frac{1}{2}$ then a noise shows an anti-persistent fractional Brownian motion (17). If $H > \frac{1}{2}$ then the noise exhibits a long term persistence and nonperiodic cycles. The Hurst noise was observed in many natural phenomena (18) and it was demonstrated in the laboratory insect populations (19), i.e. the Hurst phenomenon was reproduced in well controlled experimental conditions.

Our motivation is to better understand the emergence of power laws in the outbreak evolution, the mechanisms of spontaneous stopping of the outbreak and the nature of the noise of the daily count of infected cases $i(t)$. We were inspired by the cellular automata (20), a few features of the self organized criticality models and forest fire models (21–23). However, we had to constrain mobility of individuals and to introduce a spatio-temporal memory effect.

Experimental results

World Health Organization (WHO) provides the SARS-CoV-2 data (Supplementary Materials). We carefully selected countries: China, the Czech Republic, Belgium and Kenya (Figure 1), that show general as well as country specific features of the virus spread.

The daily count of infected cases $i(t)$ and the cumulative number of infected cases $I(t)$ (Figure 1) follow the power laws $i(t) \sim t^\beta$ and $I(t) \sim t^\alpha$, where t is a time measured in

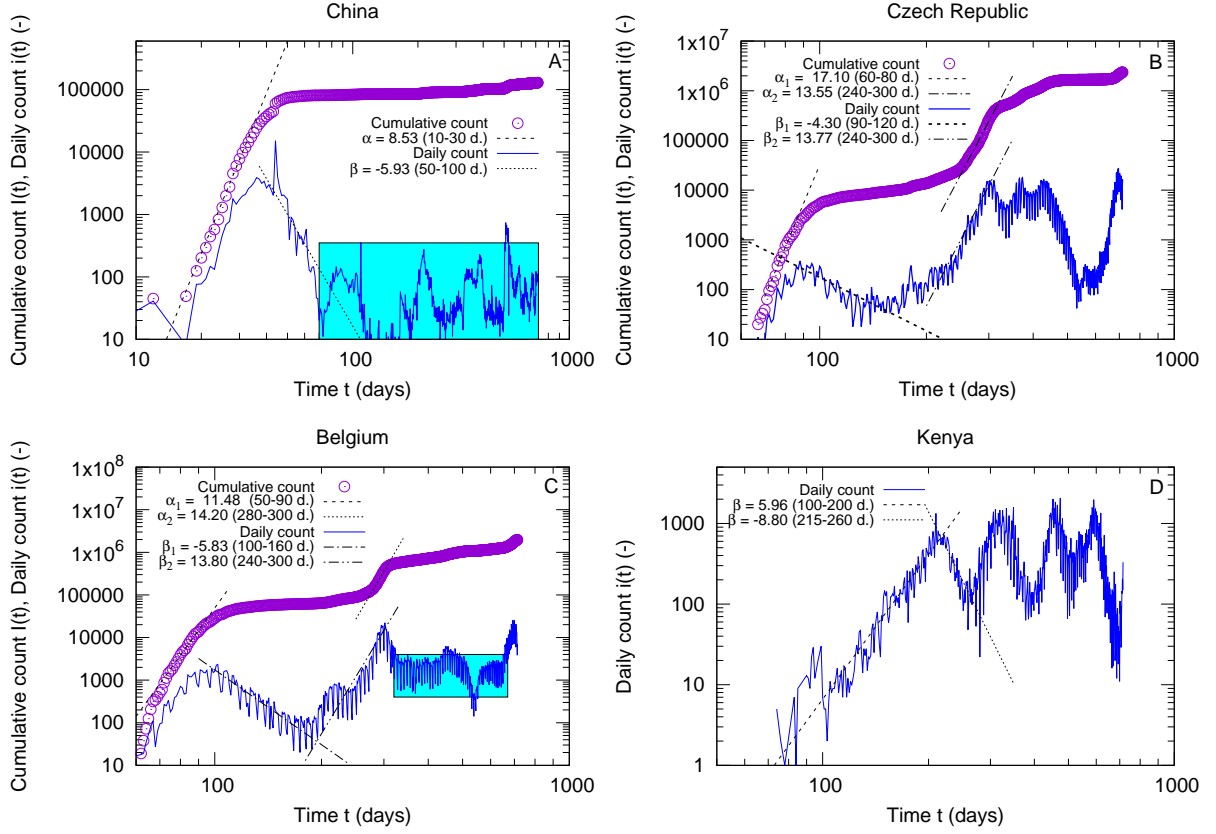


Figure 1: Power law growth of the cumulative count of infected cases $I(t) \sim t^{\alpha}$ and daily count of infected cases $i(t) \sim t^{\beta}$, where the exponents are: (A) $\alpha = 8.53 \pm 0.40$, and $\beta = -5.93 \pm 0.80$, (B) $\alpha_1 = 17.10 \pm 0.79$, $\alpha_2 = 13.53 \pm 0.25$, $\beta_1 = -4.30 \pm 0.82$ and $\beta_2 = 13.77 \pm 1.14$, (C) $\alpha_1 = 11.48 \pm 0.28$, $\alpha_2 = 14.20 \pm 0.25$, $\beta_1 = -5.83 \pm 0.63$ and $\beta_2 = 13.80 \pm 1.60$ and (D) $\beta_1 = 5.96 \pm 0.38$ and $\beta_2 = -8.80 \pm 0.8$.

days and α and β are exponents. We observed a power law growth that should be directly linked to either a decrease of mobility or other measures to prevent the virus spread. If an outbreak grows, the exponents are $5.96 \leq \beta \leq 13.80$. If the outbreak intensity declines (an outbreak decay) then the exponents are $-8.80 \leq \beta \leq -5.93$.

Outbreak dynamics in China (Figure 1 (A)) is country specific. Daily counts of infected cases $i(t)$ are low and persist to fluctuate, for a long time. This type of dynamics prevents the uncontrolled growth of outbreak size M . Rare character of the outbreak dynamics in China, i.e. these long term fluctuations of small daily counts of infected cases $i(t)$, is impossible to explain using the traditional contagion models (5–7).

Rare time series of daily count of infected cases $i(t)$ (Figure 1) are limited by the time windows of $i(t)$. Similar rare fluctuations of $i(t)$, but fluctuating around a higher value

than in the China, were observed in Belgium (Figure 1 (C)) for a long time period, more than 100 days. Generally, fluctuations of daily count of infected cases (t) are typical for all countries, for example in the Czech Republic (Figure 1 (B)) and in Kenya (Figure 1 (D)) where the fluctuations of $i(t)$ are superimposed on outbreak waves.

We evaluated the Hurst exponent H of the fluctuations of $i(t)$ for both experimental (Figure 1) and computational (Figures 2 and 3) time series (18, 19) (Supplementary Materials). The Hurst exponents H , for experimental time series of daily count of infected cases $i(t)$ (Figure 1), were found as: Figure 1 (A) $0.56 \leq H \leq 0.59$, Figure 1 (B) $0.28 \leq H \leq 0.35$, Figure 1 (C) $0.25 \leq H \leq 0.44$ and Figure 1 (D) $0.29 \leq H \leq 0.33$. In the time windows where the daily count of infected cases $i(t)$ fluctuates around a certain value, we determined the Hurst exponents H : Figure 1 (B) $H = 0.28$, for time $300 \leq t \leq 500$, Figure 1 (C) $H = 0.25$, for time $350 \leq t \leq 670$, and Figure 1 (D) $H = 0.32$, for time $200 \leq t \leq 670$.

Results of computer simulations

The computer simulations, for the constant parameters $T_i = 14$ and $l_m = 20$, and the variable parameter p , $0.130 \leq p \leq 0.140$, (Figure 2) show a power law of the cumulative count of infected cases $I(t)$, $I(t) \sim t^\alpha$ with the exponents $\alpha = 2.12$ and $\alpha = 3.19$ (Figures 2 (A) and (D)). We observed the outbreak decline (an outbreak decay) that follows the power law of the daily count of infected cases $i(t) \sim t^\beta$, with exponents $\beta = -1.98$ and $\beta = -4.74$ ((Figures 2 (A) and (D))).

Important finding is that the outbreaks can spontaneously stop their growth after a time T . We are pointing up that spontaneous stopping of outbreaks occur without a need to infect the whole population, i.e. $M \ll N$. In this growth regime, if $p < 0.140$ ((Figure 2 (A)-(C))), the duration of outbreak T and maximal count of infected cases M are random variables that span a wide interval. An outbreak (Figure 2 (A)-(C)) may stop to grow ($i(t) = 0$) and restart to grow again ($i(t) > 0$). On the other hand, the restarts of the outbreak are rare if the probability of virus transmission is $p = 0.140$ Figure 2 (D).

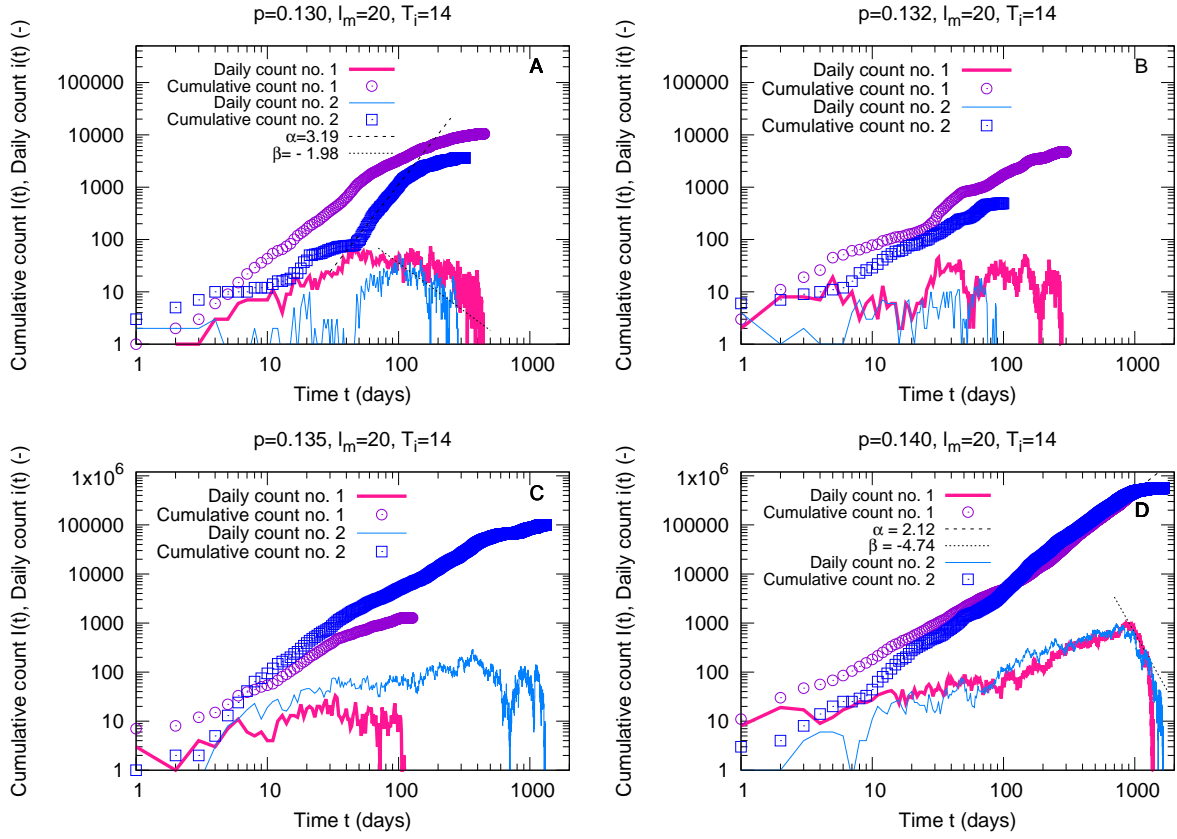


Figure 2: The computer simulations of the cumulative count of infected cases $I(t) \sim t^\alpha$ and daily count of infected cases $i(t) \sim t^\beta$, for the variable parameter p , $0.130 \leq p \leq 0.140$, and constant parameters $T_i = 14$ and $l_m = 20$.

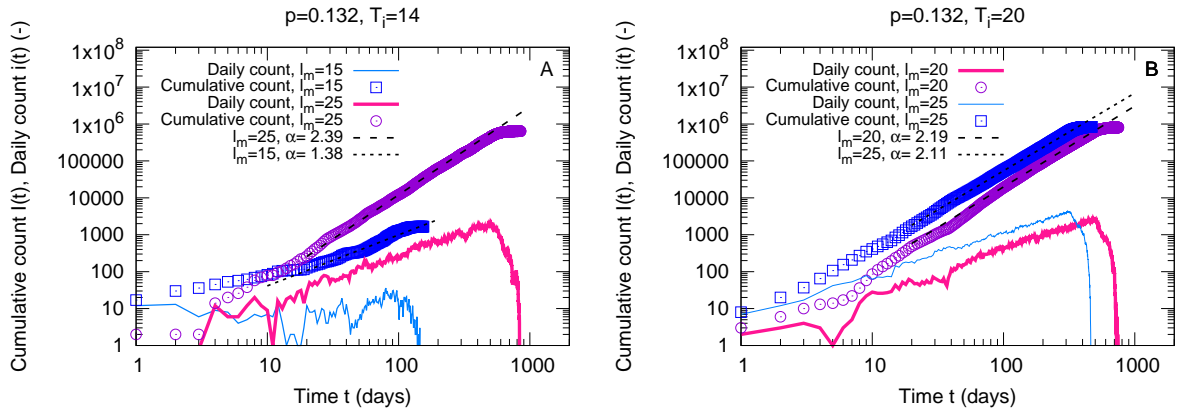


Figure 3: The computer simulations of the effect of the maximal path length l_m and duration of infected state T_i on the exponents α , on the total count of infected cases M and on the outbreak wave duration T .

If the probability of virus transmission $p = 0.132$, the duration of infection state $T_i = 14$ are constant and the maximal path length l_m decreases from $l_m = 25$ to $l_m = 15$, then the computer simulations (Figure 3 (A)) show a decrease of the maximal count of infected cases M and a decrease of the outbreak wave duration T . The decrease of the maximal path length l_m from $l_m = 25$ to $l_m = 20$, for parameters $p = 0.132$ and $T_i = 20$, has opposite the effect on the maximal count of infected cases M and the outbreak duration T . In this case, the outbreak duration T decreases and the maximal count of infected cases M increases, but $M < N$ ((Figure 3 (B))).

The computer simulations, for the parameters $p = 0.132$, $T_i = 5$ and $90 \leq l_m \leq 120$, demonstrate the effects of the maximal path length l_m on the outbreak evolution (Supplementary Materials (Figure S1)). The graphs show a decrease of the outbreak duration T that is correlated to the increase of the total count of infected cases M , if the maximal path length l_m increases.

If we ran several computer simulations, for the constant parameters $p = 0.132$, $T_i = 5$ and $l = 90$ ((Supplementary Materials (Figure S2))) we observed a complex growth dynamic. The Hurst exponents of these time series are H_m , $0.42 \leq H_{90} \leq 0.61$. We observed a random growth of the outbreaks and a change from anti-persistent to persistent fluctuations $i(t)$, probably as the effect of a change of the initial conditions and the complexity of dynamics. Such behaviors are characteristic for complex systems that exhibit chaos.

Discussion

Many species that are exposed to pathogens can alter their behaviors in ways to maximize benefits and minimize cost. Studies of social behaviors of nonhuman animals have the potential to provide important insights into ecological and evolutionary processes relevant to human health, including pathogen transmission dynamics and virulence evolution (24).

Our aim has been to implement the most important feature of animals to adapt to the pathogen enemy (24) However, we had to consider the human specific environmental

and social conditions that can dramatically change the outbreak evolution (see the model in the Supplementary Materials). The fact that the individual mobility patterns collapse into a single spatial probability distribution, indicating that, despite the diversity of their travel history, humans follow simple reproducible patterns (25) led us to implement in the model a quenched spatio-temporal mobility pattern. It is possible to identify individuals that have a high number of daily personal contacts. In the time of pandemic, social behaviors of these individuals are considered for the superspreading from an epidemiological point of view. They have a potential to infect a large number of their daily contacts (26). Superspreading skews a distribution of the reproductive numbers R (26, 27). We implemented superspreading as a variable length of daily path m that is assigned to each individual, i.e. the node $n_{i,j}$. The daily paths, m , follow a simple power law distribution (28–31) (Supplementary Materials).

A transmission of the virus from an individual to an individual we modeled as a branching process (12), where individuals can move every day along the predestined paths (Supplementary Materials), that are considered for the quenched mobility patterns (25). Recovered individuals are naturally concentrated in the spatio-temporal structures along these quenched mobility patterns. Thus the individuals create spatio-temporal barriers for the next infection contagion. We note that a transition of individuals from the infected to the recovered status represents a memory effect. In this way the evolution of the spatio-temporal distribution of recovered individuals slows down a virus spread, that can lead to spontaneous stop of virus contagion without a need to infect the whole population as it is necessary in the classical models (5–7). Individual mobility patterns of the paths of the length m , where the lengths, m , follow a power law distribution, were introduced in the model to mimic the basic social and environmental human behaviors.

The results of computer simulations show the spontaneous stopping of outbreak waves. The duration of outbreak T and maximal size of the outbreak M are random variables that span broad intervals. These quantities are independent of the population size N , $M \ll N$. Such behaviors indicate the breaking of the scaling relationships near the outbreak threshold (15). We think that the percolation phenomenon should be one of

the reasons for this broken scaling relationship. However, spontaneous stopping of the outbreak, i.e. $M \ll N$, cannot be simply explained only by considering the percolation phenomenon (32, 33), because the percolation processes are not obviously linked to the broad distributions of observable quantities. The broad range of observable values of M and T together with the spontaneous stopping of outbreak indicate that the outbreak growth process could rather resemble the avalanche dynamics a near the self-organized criticality (21, 23), if a probability of an occurrence of the outbreak of size M will follow power law $M^{-\tau}$, where τ is a scaling exponent. The proposed model, in contrast to the deterministic sandpile-like models (21, 23), has no flux of any conserved quantity.

Forest Fire Model (FFM) of Bak, Chen and Tang and Drossel and Schwabl (23), are stochastic models that are linked to percolation phenomenon (23). Natural forest fires were directly associated with the FFM (22). Our model has features of natural forest fires (22, 23), where the time evolution of forest fires is determined by the previous forest fires. This important observation has been implemented in the model as a spatio-temporal memory effect.

We unexpectedly found that the model produces the fluctuations of the daily count of infected cases $i(t)$ that show the Hurst exponents $0.29 \leq H \leq 0.95$. A signature of chaotic behaviors (Figure S2 in the Supplementary Materials) has been observed. These features of the model could be useful to explain complexity either outbreak evolution or other similar natural systems.

The strong effect of the initial conditions on the outbreak evolution enables us to understand the benefits of early mobility restrictions (34, 35) to change the outbreak dynamic (Figure S2), in comparison with the effects of the intermediate measures that are applied late, that are less intensive, that take longer time (4). For example, in the Slovak Republic and in the Czech Republic (the member states of European Union), the first SARS-CoV-2 wave has never begun as a consequence of early and strong changes of the initial conditions of the outbreak growth for a short time. However, in the next SARS-CoV-2 outbreak waves the measures were weak and long (4) that led to the full development of the outbreak waves (34), a long term dissatisfaction in society and a

dramatic increase of the deaths. After the first SARS-CoV-2 wave, the Slovak Republic reported 54 total deaths on 01. October 2020. However, one year later on 01. October 2021, before the third wave, 12660 total deaths were reported.

In summary, we have investigated a computational model of virus contagion, in which a spatio-temporal memory effect was introduced. The model generates the time series of positive numbers that show the fluctuation from the anti-persistent to persistent behaviors. A summation of these numbers follows the power law with nontrivial exponents. We unexpectedly observed a signature of chaotic behavior. A phase diagram of the model is not known, thus it should be investigated in the future. The model is possible to use in the studies of other natural phenomena that show the time series of quantities with non-trivial Hurst exponents i.e. $H \neq 0.5$. The model could be easily updated to study actual challenging tasks like reinfection, waning immunity (1), dominance of virus variants in population (2) or other natural phenomena.

References

1. J. Shaman, M. Galanti, *Science* **370**, 527, DOI 10.1126/science.abe5960, eprint: <https://science.sciencemag.org/content/370/6516/527.full.pdf>, (<https://science.sci> (2020)).
2. E. Callaway, *Nature* **600**, 204, DOI 10.1038/d41586-021-03619-8, (<https://doi.org/10.1038/> (2021)).
3. S. Hsiang *et al.*, *Nature* **584**, 262, DOI 10.1038/s41586-020-2404-8, (<https://doi.org/10.1038/> (2020)).
4. S. M. Kissler, C. Tedijanto, E. Goldstein, Y. H. Grad, M. Lipsitch, *Science* **368**, 860, DOI 10.1126/science.abb5793, eprint: <https://science.sciencemag.org/content/368/6493> (<https://science.sciencemag.org/content/368/6493/860>) (2020).
5. R. Pastor-Satorras, C. Castellano, P. Van Mieghem, A. Vespignani, *Rev. Mod. Phys.* **87**, 925, DOI 10.1103/RevModPhys.87.925, (<https://link.aps.org/doi/10.1103/RevModPhys> (2015)).

6. M. Newman, *Networks* (Oxford University Press, 2018).
7. A.-L. Barbási, *Network Science* (Cambridge University Press, 2016).
8. H. M. Singer, *arXiv:2003.11997v1*, (<https://arxiv.org/abs/2003.11997v1>) (2020).
9. S. Lai *et al.*, *Nature* **585**, 410, DOI 10.1038/s41586-020-2293-x, (<https://doi.org/10.1038/s41586-020-2293-x>) (2020).
10. C. J. Rhodes, R. M. Anderson, *Nature* **381**, 600, DOI 10.1038/381600a0, (<https://doi.org/10.1038/381600a0>) (1996).
11. R. Orbach, *Science* **231**, 814, DOI 10.1126/science.231.4740.814, eprint: <https://science.sciencemag.org/content/231/4740/814> (1986).
12. R. Antia, R. R. Regoes, J. C. Koella, C. T. Bergstrom, *Nature* **426**, 658, DOI 10.1038/nature02104, (<https://doi.org/10.1038/nature02104>) (2003).
13. S.-I. Kumamoto, T. Kamihigashi, *Frontiers in Physics* **6**, 20, DOI 10.3389/fphy.2018.00020, (<https://www.frontiersin.org/article/10.3389/fphy.2018.00020>) (2018).
14. P. D. Stroud *et al.*, *Mathematical Biosciences* **203**, 301, DOI <https://doi.org/10.1016/j.mbs.2006.05.001>, (<http://www.sciencedirect.com/science/article/pii/S0025556406000149>) (2006).
15. E. Ben-Naim, P. L. Krapivsky, *Eur. Phys. J. B* **85**, 145, DOI 10.1140/epjb/e2012-30117-0, (<https://doi.org/10.1140/epjb/e2012-30117-0>) (2012).
16. H. E. Hurst, *Nature* **180**, 494–494, DOI 10.1038/180494a0, (<https://doi.org/10.1038/180494a0>) (1957).
17. B. Mandelbrot Benoit, *THE FRACTALS GEOMETRY OF NATURE* (W.H. FREEMAN and COMPANY, 1983).
18. P. E. OConnell *et al.*, *Hydrological Sciences Journal* **61**, 1571–1590, DOI 10.1080/02626667.2015.1125998, (<https://doi.org/10.1080/02626667.2015.1125998>) (2016).
19. O. Miramontes, P. Rohani, *Proceedings of the Royal Society of London. Series B: Biological Sciences* **265**, 785, DOI 10.1098/rspb.1998.0361, eprint: <https://royalsocietypublishing.org/doi/abs/10.1098/rspb.1998.0361> (1998).

20. S. Wolfram, *Nature* **311**, 419, DOI 10.1038/311419a0, (<https://doi.org/10.1038/311419a0>) (1984).
21. P. Bak, *how nature works, the science of self-organized criticality* (Springer-Verlag, 1996).
22. B. D. Malamud, G. Morein, D. L. Turcotte, *Science* **281**, 1840, DOI 10.1126/science.281.5384.1840, eprint: <https://www.science.org/doi/pdf/10.1126/science.281.5384.1840>, (<https://www.science.org/doi/pdf/10.1126/science.281.5384.1840>) (1998).
23. G. Pruessner, *Self-Organised Criticality, Theory, Models and Characterisation* (Cambridge University Press, 2012).
24. S. Stockmaier *et al.*, *Science* **371**, 1007, DOI 10.1126/science.abc8881 (2021).
25. M. C. González, C. A. Hidalgo, A.-L. Barabási, *Nature* **453**, 779, DOI 10.1038/nature06958, (<https://doi.org/10.1038/nature06958>) (2008).
26. M. Lipsitch *et al.*, *Science* **300**, 1966, DOI 10.1126/science.1086616 (2003).
27. J. O. Lloyd-Smith, S. J. Schreiber, P. E. Kopp, W. M. Getz, *Nature* **438**, 355, DOI 10.1038/nature04153, (<https://doi.org/10.1038/nature04153>) (2005).
28. F. Liljeros, C. R. Edling, L. A. N. Amaral, H. E. Stanley, Y. Åberg, *Nature* **411**, 907–908, DOI 10.1038/35082140, (<https://doi.org/10.1038/35082140>) (2001).
29. L. M. A. Bettencourt, *Science* **340**, 1438, DOI 10.1126/science.1235823, eprint: <https://science.sciencemag.org/content/340/6139/1438.full.pdf>, (<https://science.sciencemag.org/content/340/6139/1438.full.pdf>) (2013).
30. M. Schlapfer *et al.*, *Journal of The Royal Society Interface* **11**, 20130789, DOI 10.1098/rsif.2013.0789, (<https://royalsocietypublishing.org/doi/abs/10.1098/rsif.2013.0789>) (2014).
31. M. Tizzoni, K. Sun, D. Benusiglio, M. Karsai, N. Perra, *Scientific Reports* **5**, 15111, DOI 10.1038/srep15111, (<https://doi.org/10.1038/srep15111>) (2015).
32. D. Stauffer, A. Aharony, *Introduction to Percolation Theory* (Taylor & Francis, 2003).

33. M. Sahimi, G. Hunt Allen, Eds., *Complex Media and Percolation Theory* (Springer, 2021).
34. J. Černák, *arXiv:2101.00613*, (<https://arxiv.org/abs/2101.00613>) (2021).
35. S. P. C. Brand *et al.*, *Science* **374**, 989, DOI 10.1126/science.abk0414, (<https://www.science.org>) (2021).

Supplementary Materials for

Spatio-temporal dynamics of outbreak on a lattice

with quenched mobility patterns

Jozef Černák*

December 23, 2021

Department of Nuclear and Sub-Nuclear Physics, Faculty of Science, Institute of Physics, Pavol Jozef Šafárik University in Košice, Košice, Slovak Republic

Contents

S1 Model	S2
S2 Computational methods	S3
S3 Data	S4
S3.1 Experimental data	S4
S3.2 Computer simulation data	S4
S4 Results	S6

*jozefcernak@gmail.com

S1 Model

The diffusion of individuals is defined on a two-dimensional (2D) lattice of size $L \times L$, L is a size in one dimension. An individual is assigned to the lattice node n_{ij} . The individuals create a metapopulation of the size $N = L \times L$. The individual can be mobile or immobile. The mobile individual may escape the node n_{ij} and diffuse, in contrast to the immobile individual that stands in the node n_{ij} . We define the time t . If all mobile individuals diffuse m steps from the site n_{ij} (Eq. 1) then the time t is increased by one unit $t = t + 1$. After m steps each mobile individual returns to the initial node n_{ij} (Figure S1). Mobile individuals are healthy or infected. Infected individuals are infected for the time T_i , after a time $t > T_i$, they become healthy but immobile. It is allowed only for mobile individuals to interact and transmit the infection. A movement of an individual is constrained in a step. They can diffuse only along the spatially fixed random paths of the length m , $m \leq l_m$. The parameter l_m is a maximal length of the path. For each individual n_{ij} , we define the path of the length, m , only once, at the simulation initialization. The path is a set of m nodes n_{ij} , where indices i and j are determined using the Markovian process

$$i_{k+1} = \sum_{k=0}^{m-1} i_k + a_1, \quad j_{k+1} = \sum_{k=1}^{m-1} j_k + a_2, \quad a_{1,2} = \begin{cases} 1 & 0 \leq \xi_{1,2} < \frac{1}{3} \\ 0 & \frac{1}{3} \leq \xi_{1,2} < \frac{2}{3} \\ -1 & \frac{2}{3} \leq \xi_{1,2} < 1 \end{cases}, \quad (1)$$

$i_{k=0} = i, j_{k=0} = j$, a_1 and a_2 are random integer numbers and ξ_1 and ξ_2 are uncorrelated random variables $0 \leq \xi_{1,2} < 1$ that are evaluated for each k . In simulations, the periodic boundary conditions are used to conserve a number of individuals N on the lattice. We proposed that the distribution of the path lengths m follows the power law $P_m = m^{-1}$, where $m \geq 1$ and a path length $m \leq l_m$ (see the Discussion in the main text).

Two individuals, 1 and 2, have forever defined the random paths that are shown in Figure S1. The arrows are returns of the individuals in the initial nodes n_{ij} after $m=4$ and $m = 2$ steps.

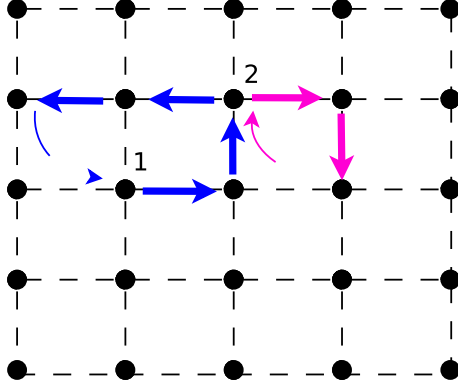


Figure S1: The random paths of the length m are generated using the Markovian process (Eq. 1). Two paths of the lengths, $m = 4$ and $m = 2$, are shown. The paths constrain a movement of the individuals, and they create a quenched disorder in the 2D lattice $L \times L$ of the size L , where $L = 5$.

A mobile individual interacts with other individuals, n_{ij} , that lie on his daily path. An infection is transmitted from infected individuals to susceptible individuals with a probability p as a branching process. The probability of infection transmission p , the infection time T_i and the maximal length l_m are model parameters.

S2 Computational methods

The computational model (Section S1) is implemented in the Python language (“m5.py” (1)). We tested the program “m5.py” using the OS Ubuntu 18.04.6 LTS. Type in the terminal: `python3 m5.py` to run a computer simulation. The program prints the time series: the time t , the daily count of infected cases $i(t)$ and the cumulative count of infected cases $I(t)$.

For plotting and fitting the experimental and computer simulation data we used a portable command-line driven graphing software the Gnuplot (2). SageMath (a free open-source mathematics software system licensed under the GPL) (3) has built the algorithm to calculate the Hurst exponent (4) as the function `hurst_exponent()`.

S3 Data

S3.1 Experimental data

World Health Organization (WHO) collects the statistics of the COVID-19 pandemic, which are publicly available in the WHO archive (5). Statistical data were downloaded from the link (6), as the comma-separated values (CSV file format). Data columns: “Date_reported”, “Country_code”, “New_cases”, and “Cumulative_cases” were exported from the Microsoft Excel data sheet “WHO-COVID-19-global-data.xlsx”. The file “WHO-COVID-19-global-data.xlsx” and exported data used to plot the graphs in Figure 1 (the main text) are enclosed in the Local Data Directories (1).

S3.2 Computer simulation data

The results of computer simulations are stored in data files “File.txt” (1). The probability of infection transmission p , the duration of infection window T_i , and the maximal path length l_m are the parameters that were used to generate the time series of $i(t)$ and $I(t)$, that are stored in data files “File.txt”. Data files and the parameters p , T_i and l_m are arranged in Tables S1 and S2. These data were used to plot the graphs in Figures 2, 3 (the main text), S2 and S3.

Data files and the parameters p , T_i and l_m are arranged in Tables S1.

p	T_i	l_m	File (.txt)	Figure 2	p	T_i	l_m	File (.txt)	Figure 3
0.130	14	20	v4	(A)	0.132	14	15	v90_5	(A)
			v40_3					v9_5	-
			v4_1	v9_3					
			v40_1	v9_4					
v40_2			v90_1						
0.132			v5	(B)			v90_3	(A)	
				v50_1			v8		-
				v5_1			v80_2		
0.135			v2	(C)			v20_2	(B)	
							v2_1	-	
	v20_1								
0.140	v1	(D)	v1_1	(B)					
			v10_2	-					
		v1							
		v10_1							

Table S1: The parameters p , T_i and l_m , and data files (“File.txt”) of the graphs in Figures 2 and 3 (the main text).

p	T_i	l_m	File (.txt)	Figure
0.132	5	90	5_90_0132	S2, S3
			5_90_0132_1	S3
			5_90_0132_2	S3
			5_90_0132_3	S3
		100	5_100_0132	S2
			5_100_0132_1	-
			5_100_0132_2	
		5_100_0132_3		
		110	5_110_0132	S2
			5_110_0132_1	-
			5_110_0132_2	
		5_110_0132_3		
		120	5_120_0132	S2
			5_120_0132_1	-
			5_120_0132_2	
		5_120_0132_3		

Table S2: The probability of infection transmission $p = 0.132$, the duration of infection window $T_i = 5$, and the maximal path lengths $l_m = 90, 100, 110$ and 120 are parameters. Data files (“File.txt”) were used to plot the graphs in Figures S2 and S3 and to determine the Hurst exponents.

S4 Results

Simulations are initiated using only one infected case, that it is placed randomly on the lattice. In such case, a probability to start an outbreak may be low (γ). We had to run the initialization of simulation many times for certain parameters. We observed a spontaneous stopping of the outbreak after the time T , for all parameters p , T_i and l_m (Figure S2), i.e. the total count of infected cases M was always smaller than a population size N , i.e. $M < N$, and $N = 1 \times 10^6$. For constant parameters $p = 0.132$ and $T_i = 5$, computer simulations (Figure S2) show the effect of an increase of l_m on the increase of the total count of infected cases M (Figure S2 (A)) and on the decrease of the outbreak wave duration T ((Figure S2) (B)).

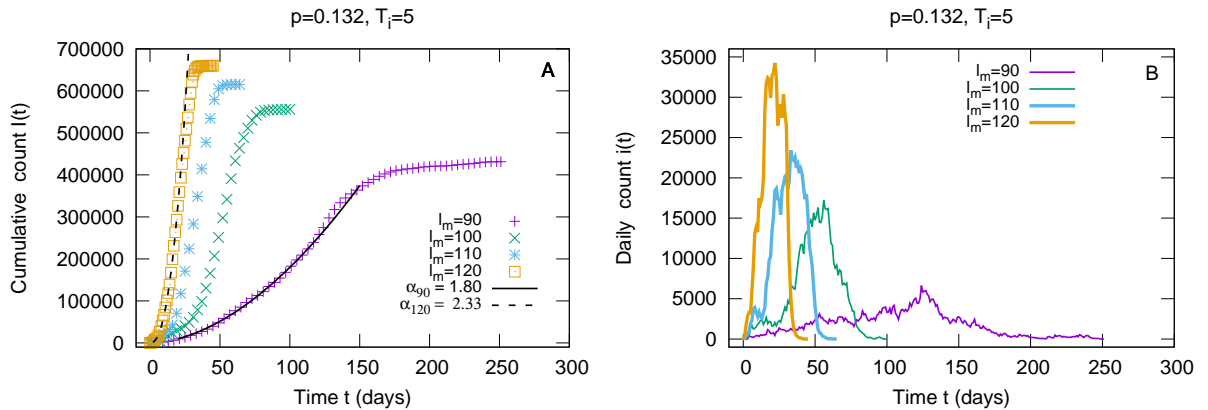


Figure S2: The computer simulations of the cumulative count of infected cases $I(t)$ (A) and daily count of infected cases $i(t)$ (B), for fixed parameters: $p = 0.132$, $T_i = 5$, and the variable parameter l_m , $l_m = 90, 100, 110$ and 120 .

We observed a stochastic growth process of the cumulative number of infected cases $I(t)$ (Figure S3), for the constant parameters $p = 0.132$, $T_i = 5$ and $l_m = 90$, that led to the spontaneous stopping of a virus contagion ($M < N$) and to the random durations of the outbreak waves, T .

We observed that, the growth of the outbreak and its decay follow the power laws $i(t) \sim t^\beta$ and $I(t) \sim t^\alpha$ (Figures S2 (A) and S3), where the exponents are $1.13 \leq \alpha \leq 2.28$ and $\beta = -5.54$.

For computer simulations (Figure 2 in the main text and Table S1), with the constant parameters $T_i = 14$ and $l_m = 20$, and the variable probability of infection transmission

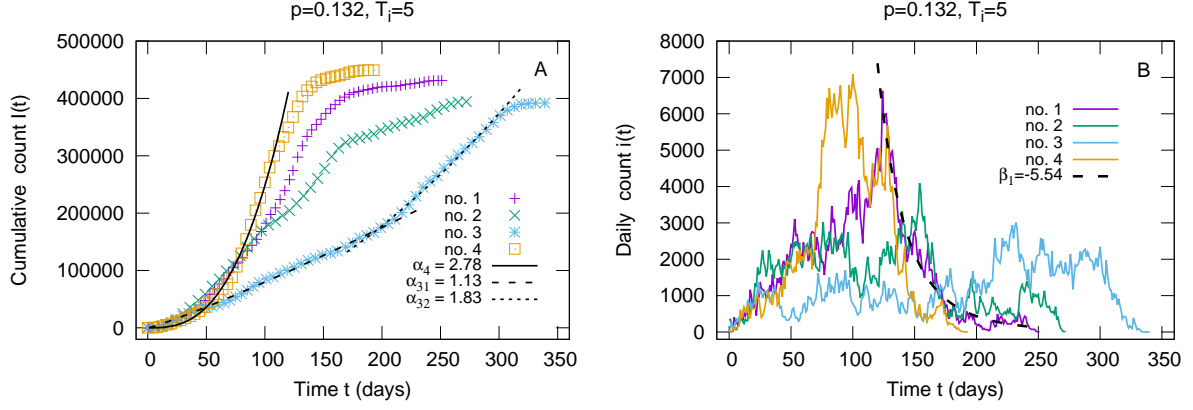


Figure S3: The computer simulations for the fixed parameters: $p = 0.132$, $T_i = 5$, and $l_m = 90$ (see Table S1). The exponents, α and β , are of the power laws $i(t) \sim t^\beta$ and $I(t) \sim t^\alpha$.

p , $0.130 \leq p \leq 0.140$, we determined the Hurst exponents H using the fluctuations of the daily count of infected cases $i(t)$ as: Figure 2 (A) $0.39 \leq H \leq 0.46$, Figure 2 (B) $0.29 \leq H \leq 0.44$, Figure 2 (C) $0.43 \leq H \leq 0.62$, and Figure 2 (D) $0.42 \leq H \leq 0.45$.

For computer simulation, with the constant probability of infection transmission $p = 0.132$ and the variable parameters $T_i = 14$ and 20 , and $l_m = 15$, 20 and 25 (Figure 3 in the main text and Table S1), the Hurst exponents H of the daily count of infected cases $i(t)$ were determined as: Figure 3 (A) $0.29 \leq H \leq 0.43$ ($T_i = 14$ and $l_m = 15$), and $0.41 \leq H \leq 0.49$ ($T = 14$ and $l_m = 25$), Figure 3 (B) $0.43 \leq H \leq 0.54$ ($T_i = 20$ and $l_m = 20$), and $0.36 \leq H \leq 0.48$ ($T_i = 20$ and $l_m = 25$).

The fluctuations of daily count infected cases $i(t)$, for parameters and data files that arranged in Table S2, have the Hurst exponents H_m : $0.42 \leq H_{90} \leq 0.61$ (a maximal duration of waves, $193 \leq T \leq 340$), $0.30 \leq H_{100} \leq 0.77$ ($98 \leq T \leq 112$), $0.44 \leq H_{110} \leq 0.95$ ($60 \leq T \leq 71$) and $0.77 \leq H_{120} \leq 0.97$ ($43 \leq T \leq 45$).

The Hurst exponents H_m of the fluctuation of daily count of infected cases $i(t)$ in Figure S2 (Table S2) are: $H_{90} = 0.55$, $H_{100} = 0.77$, $H_{110} = 0.90$ and $H_{120} = 0.77$.

References

1. J. Černák, *Local Data Directories*, <http://LDD>, 2021.

2. T. Williams, C. Kelley, *Gnuplot 5.2: an interactive plotting program*, <http://gnuplot.sourceforge.net>, 2019.
3. The Sage Developers, *SageMath, the Sage Mathematics Software System (Version 9.2)*, <https://www.sagemath.org/>, 2020.
4. E. E. Peters, *Fractal market analysis : applying chaos theory to investment and economics* (J. Wiley & Sons, New York, 1994).
5. World Health Organization, *WHO Coronavirus (COVID-19) Dashboard-Information Note*, <https://covid19.who.int/info/>, 2021.
6. World Health Organization, *WHO Coronavirus (COVID-19) Dashboard-Download link*, <https://covid19.who.int/WHO-COVID-19-global-data.csv>, 2021.
7. M. Lipsitch *et al.*, *Science* **300**, 1966–1970, DOI 10.1126/science.1086616 (2003).